UNIVERSITY OF TWENTE.

Faculty of Engineering Technology
Department of Biomechanical Engineering

Subject specific HD-EMG driven musculoskeletal modeling of the wrist for stroke subjects

Krittika Choudhury

Master Thesis
Biomedical Engineering
Document Number: BW - 691
28th August 2019

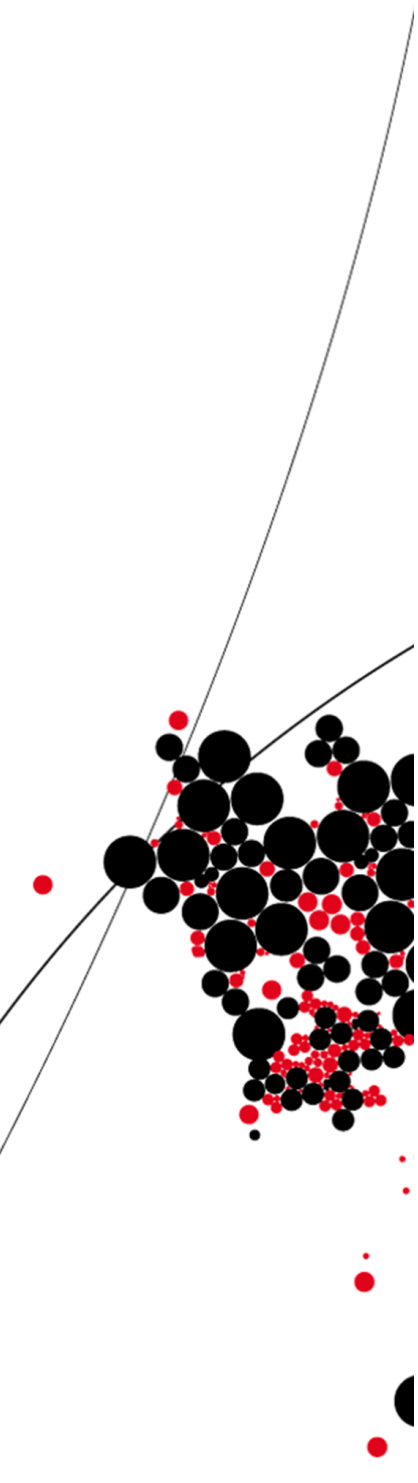

Examination Committee:
prof. dr. ir. Bart Koopman
G.V. Durandau
dr. M. Sartori
dr. U. Yavuz

Subject-specific HD-EMG driven musculoskeletal modeling of the wrist for stroke subjects

Krittika Choudhury (s1909282), Guillaume Durandau, prof. dr. ir. Bart Koopman
dr. Utku Yavuz, dr. Massimo Sartori
University of Twente, Enschede, The Netherlands

Stroke induced disabilities of the upper extremity cause significant dysfunctions at the wrist, reducing an individual's dexterity while performing activities of daily living. Limited research exists to study abnormal wrist movement patterns of stroke participants using neuromechanical modeling. Objective: Subject-specific musculoskeletal modeling of the wrist in stroke patients to help guide neuromechanical modeling strategies in the future. This study makes use of cumulative spike trains of extension and flexion generated from High Density EMG (HD-EMG) recordings of stroke patients which were decomposed using Convolution Kernel Compensation (CKC). Investigations were done to check if HD-EMG could drive the musculoskeletal modeling pipeline and if this previously tested modeling approach could work with neural and kinematic inputs from stroke patients. Methods: A subject-specific musculoskeletal model of 6 muscles and one degree of freedom, wrist flexion-extension was used in this study. The model was driven using decomposed HD-EMG recordings. Results: The subject-specific HD-EMG driven musculoskeletal model was validated for four stroke subjects on the basis of torque estimation and transformations estimated by the model, such as activations and muscle forces. Comparisons were done across all cycles for each trial of a participant, as well as across all trials of each participants. Conclusion: Results show that for stroke participants, the model estimated torques were well-correlated with the experimental torques in terms of shape and magnitude.

***Index Terms*—EMG driven musculoskeletal modeling, wrist, HD-EMG, stroke patients, neural toolbox, Convolution Kernel Compensation**

I. Introduction

Musculoskeletal systems in humans are highly redundant. This poses a challenge in the study of human motor control as it is extremely difficult to determine which muscles are activated to produce certain movements [1]. This challenge is even more palpable in case of abnormal movement patterns such as those seen in stroke patients. Approximately 70% to 80% stroke patients are limited in their ability to carry out activities of daily living (ADL) due to motor impairment of the more affected upper limb. Functional independence of 50% to 70% stroke survivors is limited by arm disabilities at the wrist, elbow or shoulder joint, post stroke [2].

The structural complexity of the wrist allows changes in the orientation of the hand to perform required tasks. Wrist movements occur around two main axes, flexion-extension and abduction-adduction (Appendix A). Neurological and orthopaedic impairments lead to inevitable dysfunction in the movements of the hand and the upper extremity [3]. Limited studies exist to understand post-stroke wrist movement abnormalities, as compared to the proximal part of the upper limb, such as the shoulder and the elbow. Current musculoskeletal models prove to be rather primitive in case of post-stroke participants. Moreover, most of these models make use of numerical coefficients based on arbitrarily assigned muscle significance factors and approximations of only the arm and shoulder in planar movements [4].

Best practices dictate that knowledge of internal forces and moments are vital to design neuromuscular and rehabilitation strategies [5]. However, acquiring in-vivo measurements of variables, such as muscle force, is impractical because of its invasive approach. Electromyography (EMG) driven musculoskeletal modeling does not suffer from the same limitations as recorded EMG, and kinematic input such as muscle tendon length is used to determine muscle forces directly. EMG driven models have previously been used to analyze movement patterns in healthy subjects, especially for lower extremities [6][7]. In [8] and [1], the reader can find examples of cases where EMG driven modeling has been applied to the upper extremity. However, this approach has not yet been applied to the wrist, especially in the case of post-stroke patients. Therefore, this lends novelty to our study in many ways.

First of all, the biomechanical models are scaled according to subject specifications for all four stroke participants. Secondly, high density EMG (HD-EMG) is used as the neural input to the modeling pipeline instead of EMG envelopes. Finally, this approach is being tested using data from the upper

extremity of post stroke patients. The findings of the study establishes that the EMG driven modeling pipeline used in the study, is adaptable, irrespective of the kind of tasks, neural input and muscles under consideration. This study also helps to understand the benefits of using HD-EMG recordings over more prevalent kinds of EMG in case of stroke participants. Most importantly, conclusions from this study can be used to design more subject-specific, robust rehabilitation and neuromuscular strategies for the wrist joint in stroke participants.

A. State of the Art - Musculoskeletal Modeling

Musculoskeletal modeling has been used actively to quantify biomechanical output and activities. It has made non-invasive methods of observing muscle and joint function during dynamic activity possible [9]. Investigations done on musculoskeletal models have opened up newer avenues of research to study the effect of muscles on joint kinematics and moments. The modeling process involves the use of kinematic data from passive or active markers placed on the body.

These models mostly use a Hill-type muscle model and allow research on treatment and rehabilitation possibilities of joints. In [10], the reader can find studies focused on creating dynamic models for the upper extremity, that included the elbow, forearm, and the wrist. Properties such as moment arm values, muscle geometries and force generation are essential to establish the accuracy of musculoskeletal models [11]. In studies conducted in [12], [13] and [14] musculoskeletal models of varying elbow and forearm positions have been used to establish moment arms as functions of joint angles in upper limb muscles responsible for wrist flexion-extension.

Software packages such as OpenSim and Anybody allow the possibility of inverse dynamics and kinematics on experimental data offline using generic and openly available models that can be scaled according to subject specific anthropometric data [15][16]. Broadly, all musculoskeletal modeling platforms use one of either two types of optimization to solve redundancy in movement biomechanics, namely, static or dynamic optimization and optimal control theory. OpenSim for example, uses a static optimization criteria to determine distribution of forces and muscle activation during a particular motion, such as, minimal metabolic cost of transport [17]. Static optimization is computationally faster than dynamic optimization, but cannot provide reliable simulations for models during tasks such as vertical jumping.

The reader can find examples of musculoskeletal models of the wrist adapted on OpenSim for studies conducted in [18] and [19]. However, these studies were focused mainly on isometric tasks, specific pathologies and tests were done on healthy participants with artificially generated tremors at the wrist joint. The muscle force patterns estimated in this approach are valid for specific conditions. However, the optimization approach used to arrive at the estimates ignores the non-linear and context dependent dynamics of the neuromuscular system [17].

B. State of the Art - EMG recordings and decomposition

For the longest time, intramuscular recordings were used for the investigation of individual motor unit properties. This method is invasive and therefore, cumbersome. Surface EMG recordings is another prevalent method of recording EMG activity and classical surface EMG is modeled as interference signals. Spatial filtering and spatial sampling can be adopted to identify individual motor units from surface EMG recordings However, the primary problem of surface EMG decomposition is to establish its accuracy [20][21].

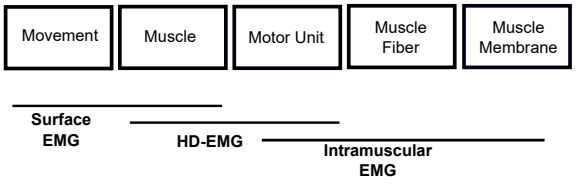

Figure 1: Scope of prevalent EMG techniques adapted from [22]. Surface EMG is mainly used for movement studies, HD-EMG gives information at the motor unit level, and intramuscular EMG gives information at the muscle-fiber level

In HD-EMG recording systems, a grid of electrodes sample the muscular activity over large surface areas. It is a non-invasive method to record temporal as well as spatial EMG activity. HD-EMG decomposition is necessary to identify discharge patterns of motor units (MU) that significantly contribute to action potentials and also for the investigation of stretch reflexes [20]. Figure 1 gives a pictorial representation of the scope of prevalent EMG types.

Reliable detection of MU behaviour has been suffered from constraints such as accuracy, invasiveness and computational complexity (Appendix D). Blind source separation is one of the most commonly employed methods of HD-EMG decomposition. This method does not rely on prior knowledge and is not sensitive to the estimation or superimposition of action potential shapes [23]. The performance of this method is limited when there is an increase in motor unit synchronization [20].

In [21] and [24], the accuracy of the Convolution Kernel Compensation (CKC) based MU identification method for HD-EMG decomposition was established for both pennate and parallel-fibred muscles at low force contractions. The accuracy of the CKC decomposition method (91.5±5.8%) has been found to be comparable to intramuscular (95±5.6%) recordings. The discharge patterns of MUs identified by both types of recordings were similar for different levels of contraction [24]. CKC estimates the discharge pattern of individual motor units and not the underlying mixing process, therefore, reducing the computation time significantly [20][25]. It adopts Bayesian optimal linear minimum mean square error estimators, is significantly noise resistant and is applied to cross correlated signals [20][24]. The Pulse to Noise Ratio (PNR) metric was subsequently introduced to estimate the accuracy of decomposition. The PNR measure showed significant correlation with both sensitivity and false alarm rate of MU discharges for 5% to 70% maximum voluntary contractions and signal to noise levels ranging from 0 to 20 dB. Experiments were conducted in [23] and [26] where 97% of the pulse was successfully reconstructed upto 5 dB of SNR and discharge patterns of motor neurons were detected accurately using the PNR measure. PNR was found to be $\geq$ 0.9 for all decoded MU and contraction levels, respectively.

There still exists a few limitations in adopting CKC for HD-EMG decomposition, such as, inferior performance in the case of ill conditioned signal mixtures [20]. Time localization of underlying signals is also ignored in this approach [23]. Accuracy and yield of HD-EMG decomposition has been found to reduce with an increase in muscle activity and decrease in SNR. The most important disadvantage of CKC is the universal assumption that it can only be applied to relatively low contraction forces [25].

C. EMG driven musculoskeletal modeling

EMG driven musculoskeletal modeling has been found to have a few clear advantages over regular musculoskeletal modeling. Variables such as muscle force cannot be estimated experimentally. EMG driven musculoskeletal modeling allows the estimation of internal variables of the body using EMGs and marker data. In this forward dynamic modeling approach, a combination of EMGs and numerical simulations are used to account for neuromuscular strategies. Making assumptions on muscle recruitment is, therefore, avoided in this approach [27]. It has constantly been suggested to allow participants to perform a range of complicated tasks to judge the performance criteria of this approach [28].

Most existing studies make use of envelopes of surface EMG for neuromechanical modeling [6][29]. Decomposed HD-EMG has also been successfully incorporated in this modeling approach to measure stiffness during isometric tasks and also, to decode casual motor neuron behaviour [26]. However, this modeling approach has mostly been adopted for wrist and hand prosthesis in the case of phantom-limbed or healthy participants [30].

Adapting this approach to stroke patients could inspire new neuromechanical modeling and rehabilitation strategies. Task training and rehabilitation could significantly improve the quality of movements in stroke patients.

D. Aim of the Project

In this project, subject-specific HD-EMG driven musculoskeletal modeling was attempted for four stroke patients. To this end, cumulative spike trains from wrist extensors and flexors were used as the neural input to the musculoskeletal modeling pipeline. These cumulative spike trains were achieved by identifying MUs from HD-EMG recordings using the CKC decomposition method. Wrist flexion and extension data was fed as kinematic inputs to the pipeline. The validity of the approach was tested on all trials of four stroke participants. The model estimations made by the HD-EMG driven modeling approach in the case of stroke patients was also compared with healthy patient data from literature.

II. Method

A. Data collection

Experimental data was recorded from five different post-stroke participants, test subject 1 to test subject 5. Data from test subject 4 could not be included in the study as the stroke patient did not return for successive trials. Five sessions were recorded with each patient over five different days. The only exception was made for the first participant where all five sessions were recorded on the same day. In each session, eight trials were carried out on average for each participant. All of the wrist flexion and extension tasks were done with the Universal Haptic Drive (UHD), a rehabilitation robotic device which typically allows two degrees of freedom; planar arm movement with its ARM mode and wrist flexion-extension and forearm pronation-supination with its WRIST mode [31].

The experimental task that the participants had to perform was wrist flexion-extension. Two arrays of 5x13 electrodes (from OT Bioelettronica, Torino. Italy) were used to record HD-EMG signals. These

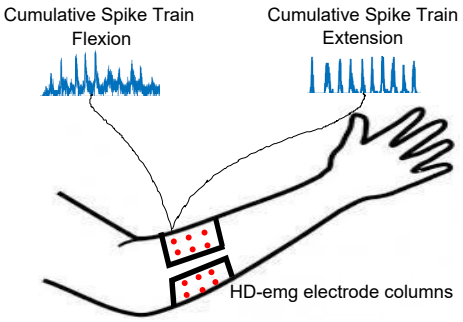

Figure 2: HD-EMG electrode grid placement

HD-EMG electrode columns were positioned circumferencing the arm, to record muscle activity from all extensors and flexors of the wrist. HD-EMG grid placement around the arm and the cumulative spike train patterns can be seen in Figure 2. Recorded HD-EMG activity was decomposed using CKC to identify MUs responsible for wrist extension and flexion activities.

The target for muscle excitation level was set at either 10% or 20% of the possible maximum voluntary contraction (MVC) for all participants. The maximum excitation level was set to 10% on the UHD and visual feedbacks were sent during tasks to let participants know if they met the target excitation level [31]. Tasks were repeated about 10 times for each participant with a rest period of 10 seconds between tasks. The dynamic flexion-extension tasks were designed such that they could exceed this target level of 10% and maintain the exceeded level of muscle excitation for at least 2 seconds. Figure 3 represents the positioning of the wrist during data collection and the graphical feedback sent to the participant in the form of the black dashed line.

B. Data Preparation

The dynamic tasks were recorded at a sampling frequency of 2048 Hz and all other data was synchronized with data from UHD. Torque data existed in separate files for flexion and extension in normalized units such that the maximum value was 10 Nm/rad. Deviation and flexion torque were recorded in the horizontal and vertical directions, respectively. Positive radial deviation and negative ulnar deviation were parameters measured in the horizontal direction. Wrist flexion torque was negative and measured in the vertical direction along with positive wrist extension.

The maximum range of motion for flexion and extension was 90°. The range of motion was validated on OpenSim visually. Joint position was

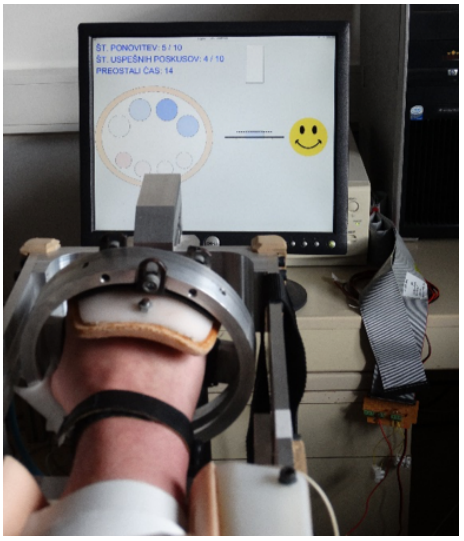

Figure 3: Graphical feedback during wrist flexion where the maximum muscle target excitation level was set to 10% [31]

Cumulative spike trains	Muscles	Abb.
CST_FLE	Flexor carpi radialis	FCR
CST_FLE	Flexor carpi ulnaris	FCU
CST_FLE	Flexor digitorum superficialis	FDSR
CST_EXT	Extensor carpi radialis longus	ECRL
CST_EXT	Extensor carpi radialis brevis	ECRB
CST_EXT	Extensor carpi ulnaris	ECU

Table I: HD-EMG to MTU mapping

also plotted with respect to the muscle tendon unit (MTU) lengths to avoid data misinterpretation.

HD-EMG decomposed using CKC was used to identify relevant MUs and generate two cumulative spike trains; wrist extension (CST_EXT) and wrist flexion (CST_FLE). CST_EXT was used to activate the three extensor muscles, and CST_FLE was used to activate the three flexors. Table I represents the spike train to MTU mapping used in this study.

The cumulative EMG spike trains were filtered using a 4th order Butterworth filter and Matlab's filtfilt function [32][33]. A cutoff frequency of 2 Hz was chosen as the flexion-extension movements were rather slow. Only these filtered cumulative spike trains were used further in this project. After a few initial trial routines routines, it was established that filtered HD-EMG gave better results.

Normalized HD-EMG for flexion and extension was computed from the set of all trials of each participant [6]. From all trials of each participant, the maximum HD-EMG amplitude for flexion was used as the normalization reference for flexion. Similarly, the maximum amplitude of HD-EMG for extension was used as the normalization reference for extension for all trials.

All three kinds of data files were too large which caused lags and longer computation times. To this

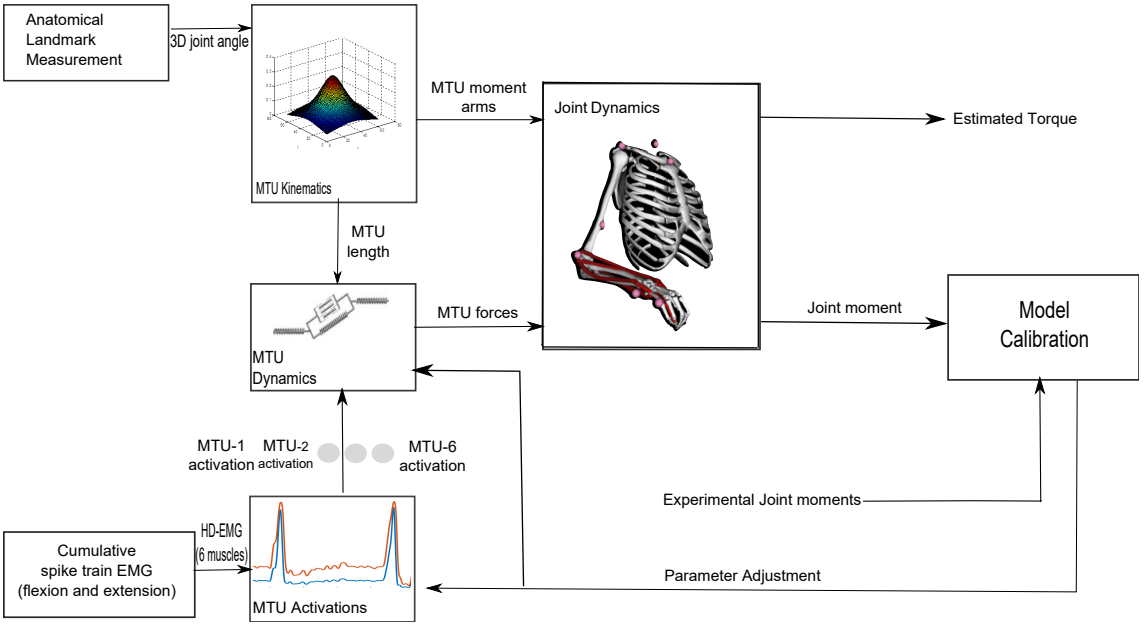

Figure 4: Schematic diagram of the HD-EMG driven musculoskeletal modeling pipeline used in the study. Each block has been explained in detail in the II-C: HD-EMG driven musculoskeletal modeling. This schematic diagram is an adaptation of [6].

end, data from all trials was resampled at 100 Hz. Thus, resampled torque, joint position and HD-EMG activity data were used as inputs for the HD-EMG driven musculoskeletal modeling pipeline. Only one degree of freedom (DOF), wrist flexion-extension was investigated during this project.

C. HD-EMG musculoskeletal modeling pipeline

The open-source biomechanical modeling software Opensim [15][34] and the open-source toolbox CEINMS were used to estimate the wrist joint kinematics [35]. These platforms were also used to estimate various MTU properties such as activations, muscle tendon lengths, and moment arms. A detailed description of this musculoskeletal modeling pipeline can be found for the lower extremity in [36]. This pipeline has been adapted for the upper extremity in this project in Figure 4. The key aspects of the methodology have been summarized in this section.

- MTU activation block: Cumulative spike trains decomposed from HD-EMG activity recorded from the extensors and flexors of the wrist were mapped into activations α(t). The mapping sequence in Table I was used to drive the six MTUs.
- MTU kinematics block: A generic model of the MoBL ARMS dyamic upper limb [37] with six MTUs was scaled on OpenSim for each participant. The elbow flexion and pronation-supination coordinates are set to 90°, such that the position of the arm matched the experimental conditions. Changes are seen only in the flexion and deviation movements. The anatomical position of the arm and hand were taken for all subjects. Scaling of the model was therefore done using manual scale factors for each participant. The MTU lengths(l^{MTU}) and flexion moment arm (r) obtained from OpenSim were fed into the CEINMS toolbox.
- MTU dynamics block: In this block, activations α(t), l^{MTU} and contraction velocity v^{MTU} were used in conjunction to compute MTU forces (F^{MTU}). F^{MTU} is given by the equation corresponding to a Hill Type muscle model,

$$F^{MTU} = F^t = F^m cos(\phi(l^m)) = [\alpha(t) f(\tilde{l}^m) f(\tilde{v}^m) + f_p(\tilde{l}^m)] F^{max} cos(\phi(l^m)) \quad (1)$$

  In equation 1, F^{max} represents maximum isometric muscle force, $\tilde{l}^m$ and $\tilde{v}^m$ represent fiber length and velocity normalized to optimal fiber length, respectively. MTU force equals both tendon force, F^t and muscle fiber force, F^m since they are in series [6].
- Calibration block: The HD-EMG driven musculoskeletal model had to be calibrated before it could be run in open loop for the prediction of joint torques and muscle forces. In this block of the pipeline, certain subject specific model parameters were adjusted using an optimization routine. The model parameters that got adjusted were the three coefficients that

describe the non-linear muscle activation dynamics, i.e. the slack length, the optimal fiber lengths of the modeled muscles and a strength coefficient for each MTU. [6] explains the model parameters in detail for the ankle and knee joint. An adaptation of this explanation is used in this study for the upper extremity, and more specifically, the wrist joint. The objective of the optimization routine is to minimize the difference between the estimated torque and the recorded experimental torque. Therefore, a pre-requisite to run this optimization procedure is to know the experimental torque for flexion and deviation of the wrist joint. In our case, these were already recorded during the data collection process. Calibration was done on two trials which had comparatively higher flexion and extension activity. The results from this calibrated model were extrapolated to all trials of that participant.

D. Data analysis

For the ease of data visualization and analysis, cycles of all trials were extracted and all data were interpolated and time-normalized using cubic splines [38]. Each cycle was defined as a complete period of the torque profile from minimum to minimum. The HD-EMG driven model was validated at the torque level. Flexion torques estimated by the model were compared to the experimental torques obtained during data collection using the UHD for wrist and arm movement rehabilitation. Results were compared in shape using the Pearson correlation coefficient, R. Results were also investigated in magnitude by calculating the root mean square error (RMSE) between the input experimental and model estimated output torque. A thorough visual check was done especially for stroke or test participants. To that end, model transformations were plotted against each other. Cumulative spike train excitation to activations, activations to muscle forces, and muscle forces to estimated model torque were a few of the plots made separately for both flexor and extensor groups. Finally, flexion averages of both the experimentally recorded torque and model estimated torque were plotted and their Pearson correlation coefficient and RMSE were calculated to compare their shapes and magnitude. Torque validation comparisons were done for each trial and also for all trials of each participant.

III. Results

A. Transformations made by the model - Estimated parameters

The EMG mapping and the CEINMS model transformations are validated in this section. It is expected that the joint torques and muscle forces best match the cumulative spike trains of flexion-extension EMG generated from experimentally recorded HD-EMG. The cumulative spike train input is mapped to the activations estimated by the model, followed by a mapping of the estimated activations to estimated muscle forces. Finally, the estimated muscle forces are compared with the estimated model torques to check for inconsistencies. Model transformations were mapped separately for the flexor and extensor muscles. Figure 5 gives an idea of the transformations made by the model.

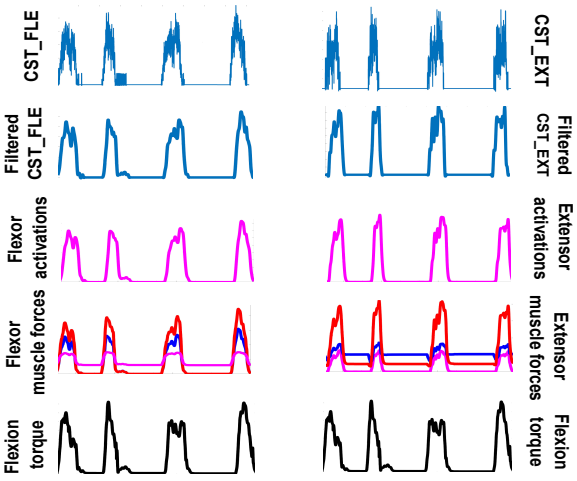

Figure 5: Transformations made by the HD-EMG musculoskeletal modeling pipeline

One trial of the third subject had to be excluded from the study as there was no noticeable extension EMG activity. This could have been due to errors in HD-EMG recording or decomposition. Table II gives the mean and standard deviations of the muscle parameters as estimated by the HD-EMG driven musculoskeletal modeling pipeline for all cycles of one trial for each participant. It is seen that the flexors in general have higher activations and muscle forces than the extensors. And the primary wrist flexor (FCU) and wrist extensor (ECRB) have higher muscle forces than the other muscles.

1) Flexor-Extensor muscle activity

Figure 6 investigates the activity of all three flexors, FCU, FCR and FDSR averaged over all cycles of the trial, for three representative trials of participant 1. Similarly, the activity of the three extensors is investigated in Figure 7. The filtered cumulative spike train for flexion and extension were used to activate the flexor and extensor muscles, respectively. Therefore, in each trial, all three flexors were equally activated (meaning they had the same value for activation in normalized units) and all three extensors were equally activated. The first subplot of Figures 6 and 7 maps the CST to this

Sub.	Activations (norm. units)		Muscle forces (in N)						Exp. torque (in N.m)	Est. torque (in N.m)
	extensors	flexors	ECRL	ECRB	ECU	FCR	FCU	FDSR		
Sub. 1	0.012±0.02	0.45±0.3	1.91±3.2	1.13±2.2	1.49±2.5	50.29±39.1	29.09±24.8	12.47±10.3	1.28±0.5	1.45±0.8
Sub. 2	0.10±0.06	0.41±0.2	4.52±2.1	25.09±2.7	111.57±22.1	30.71±5.9	118.76±63.4	13.92±2.2	2.35±1.3	1.69±1.0
Sub. 3	0.17±0.16	0.43±0.3	17.6±16.3	51.23±11.3	73.87±49.5	80.09±62.4	112.25±91.3	56.43±17.2	2.25±1.3	1.59±1.3
Sub. 5	0.11±0.08	0.35±0.3	72.23±34.3	225.4±29.3	27.87±8.1	135.7±34.8	175.08±46.3	61.6±13.4	1.64±0.9	1.79±1.3

Table II: HD-EMG driven modeling estimations of muscle parameters

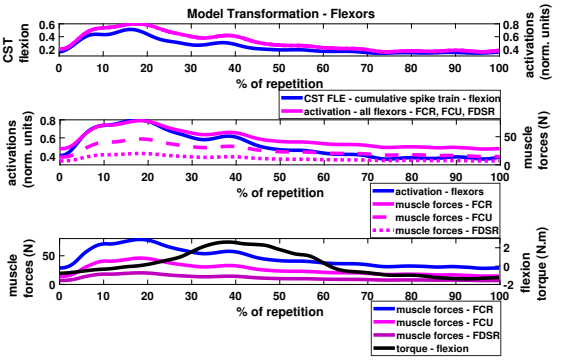

(a)

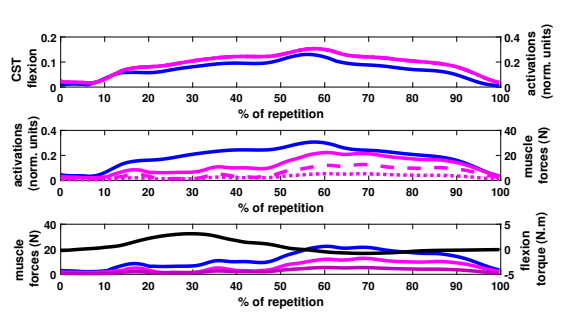

(b)

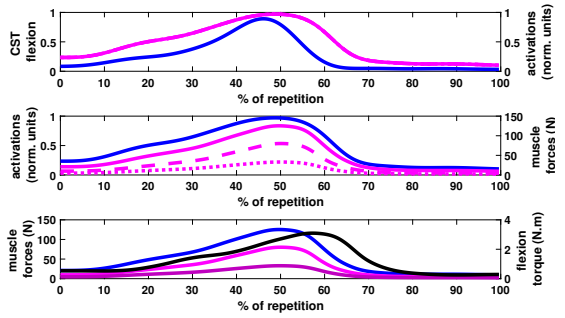

(c)

Figure 6: Flexor muscle activity of the first, fourth and fifth trials of stroke participant 1 are given by 6a, 6b and 6c respectively, mapped sequentially from filtered flexion cumulative spike train to estimated flexion torque

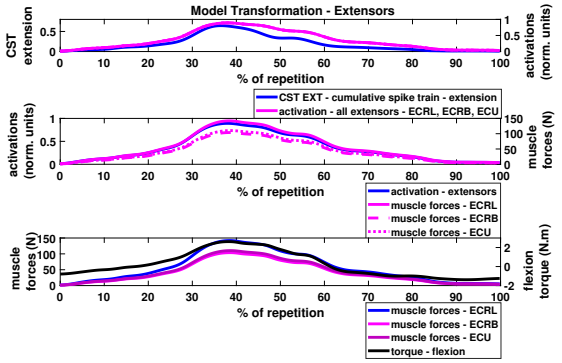

(a)

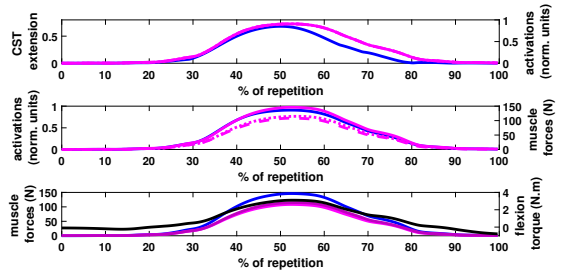

(b)

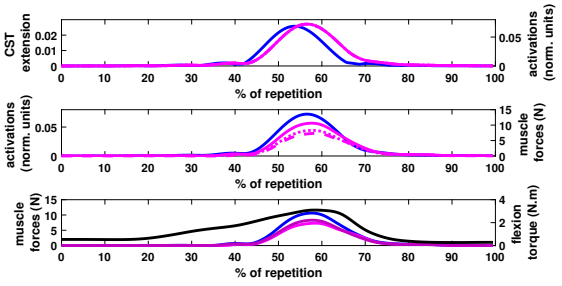

(c)

Figure 7: Extensor muscle activity of the first, fourth and fifth trials of stroke participant 1 are given by 7a, 7b and 7c respectively, mapped sequentially from filtered flexion cumulative spike train to estimated flexion torque

activation (in normalized units). The parameters of the model such as shape factor and activation scale were 1. Activations and experimental torques were used to estimate MTU forces. Therefore, activated flexors/extensors were mapped to estimated MTU forces (in N) in the second subplot of both figures. Finally, in the third subplot of Figures 6 and 7, the estimated MTU forces (in N) and estimated model flexion torques (in N.m) were mapped to each other to validate the extent of parameter adjustment.

B. Torque level

All the tasks performed during this experiment were dynamic, and results shown here are from all four post-stroke participants. The dynamical consistency of the HD-EMG driven musculoskele-

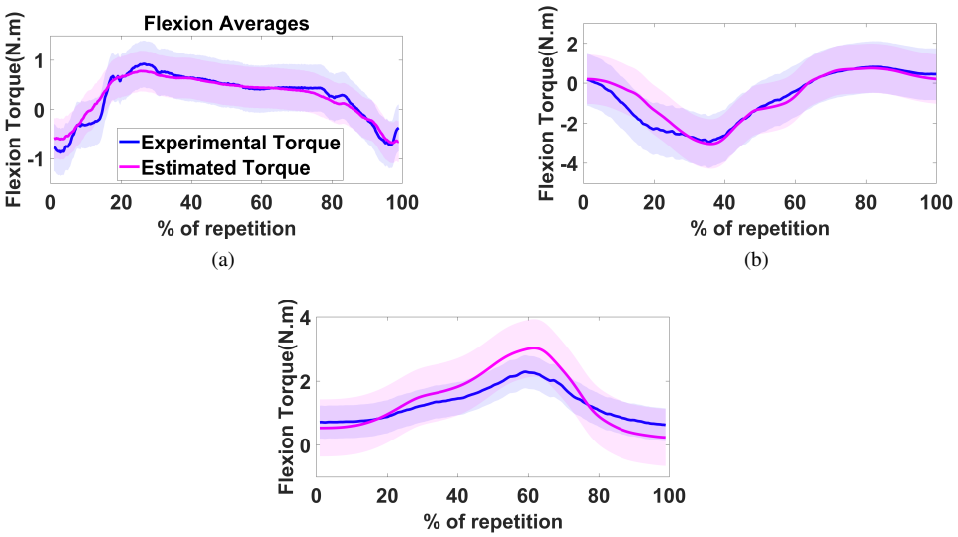

Figure 8: Flexion averages of the experimental torques and estimated model torque of three representative trials of the first participant. The magenta and blue lines represent estimated model torques and experimental torques respectively. The shaded region represents the standard deviation of the experimental and estimated torques. 8a shows the first trial (R 0.947, RMSE 0.0029 N.m) to which the calibrated model was extrapolated. The std. dev. of the experimental torque is 0.4775 whereas it is 0.4148 for the estimated torque. Calibration was done on the fourth and fifth trials represented by the second and third subfigures. 8b represents the fourth trial, (R 0.9555,RMSE 0.1050 N.m) the std. dev. of the experimental torque and estimated torques are 1.2965 and 1.2342 respectively. R and RMSE values for the fifth trial, represented by 8c are 0.1708 and 0.9888 respectively. The std. dev for experimental torque is 0.5156 whereas it is 0.8935 for the estimated torque

tal modeling pipeline was validated by comparing experimental torques with the estimated model torques.

1) Torque comparison for individual trials

For each of the four post-stroke subjects, the calibration was done on two trials and this calibrated model was extrapolated to all trials of that subject. Across all 92 cycles, RMSE and R values were used as indicators of goodness of fit of the experimental and model-estimated values of flexion torque. Pearson correlation values, R, ranged from 0.8905 to 0.9888. RMSE values ranged from 0.0029 N.m to 1.5624 N.m. The last two trials (7th and 9th trial) of the first subject had deviant R and RMSE values. The seventh trial had an RMSE of 5.3 N.m with an R value of 0.1095, whereas the ninth trial had an RMSE of 2.8092 N.m with an R value of 0.7623. This was because the maximum experimental flexion-extension torque of these two trials were much higher even though their joint position data and EMG activity values were comparable to the other trials. For example, maximum experimental flexion torque for the seventh and ninth trials of the first subject fell in the range of 9.0-10.4 N.m. whereas the maximum flexion torque for all the the other trials were in the range of 0.28 to 4.60 N.m. This could have led to underestimation of flexion torque by the model for these two trials. The sixth trial of the fifth test subject had a deviant R value of 0.3326, as the model took mainly the ECRB muscle force into account to estimate the flexion torque, which was much higher than the other extensor muscles. Figure 8 gives a comparison of flexion averages over all cycles for experimental and estimated torques. Appendix F has RMSE and R values, as well as plots of experimental vs. estimated flexion torque for each trial of all four participants.

2) Torque comparison across trials for every participant

The averages of all trials were also taken in case of each participant to evaluate the RMSE and Pearson correlation of the experimental and estimated flexion torques for the participant as a whole. Trials seven and nine of participant 1 were excluded from the this average because of their comparatively high experimental torques and low model estimated torques. On comparison of averages of experimental and estimated torques across all participants, it was found that the R value for all participants were in the range of 0.9601 to 0.9933, with RMSE values ranging from 0.54 N.m to 3.17 N.m. 3.17 N.m was the RMSE value for participant 3, here flexion torque values were comparatively much higher for the sixth trial (15.4 N.m) while the other trials had experimental flexion torques in the range 2.4 N.m to 7.6 N.m. Figure 9 gives standard deviations, RMSE and R values

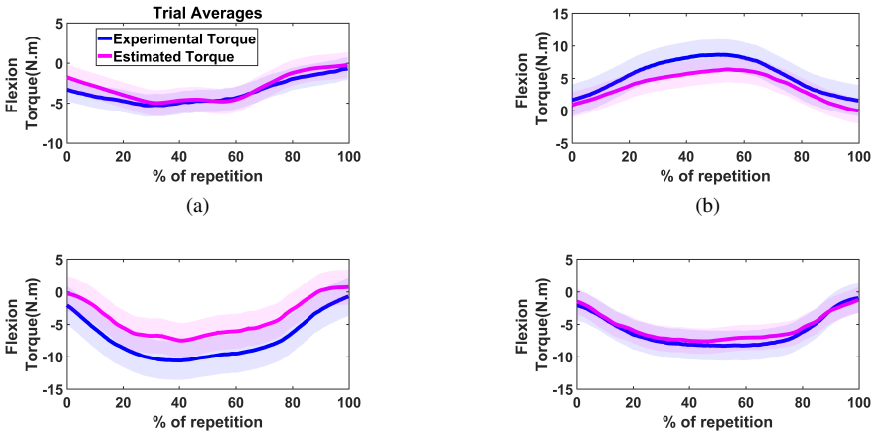

Figure 9: Flexion averages of all trials were calculated for each participant. The blue and magenta lines represent experimental and estimated torques respectively, the shaded area around them represents the standard deviation of both torques. 9a gives the trial average graph for participant 1 (RMSE 0.5360N.m, R 0.9601) where the std. dev. of exp. torque was 1.40 and std. dev. of estimated torque was 1.59, 9b represents participant 2 (RMSE 1.6593N.m, R 0.9875) with a std. dev. of 2.41 in exp. torque and 1.96 in estimated torque, 9c represents participant 3 (RMSE 3.1783N.m, R 0.9933) with a std. dev. of 2.98 and 2.69 in exp. and estimated torques, respectively, and 9d shows trial averages for participant 5 (RMSE 0.5436N.m, R 0.9933) where the std dev. for exp. and estimated torque were 2.3 and 1.95, respectively

across all trials for each participant.

IV. Discussion

In this project HD-EMG driven musculoskeletal modeling was applied and validated for post-stroke participants. EMG to muscle mapping showed that all transformations by the model and the estimated model torques were validated in terms of shape as well as magnitude. It was established that the model was dynamically consistent and gave satisfactory estimates of joint torque.

Cumulative EMG spike train for both flexion and extension were filtered using a cutoff frequency of 2 Hz. It is a possibility that using the same cutoff frequency for both flexion-extension spike trains and for all trials of each smoothing window lengths, might have led to some loss in important EMG information. EMG amplitudes are also dependent on the kind of task and joint position, which might limit the accuracy achievable by an EMG driven model [39][40].

Studies have shown that HD-EMG grids estimate force 30% better than bipolar electrodes, and other conventional methods. Collection surface has also proven to be the singular most important factor in electrode configuration. Larger collection surfaces depict estimations of better quality by about 25% [41]. During data collection, HD-EMG grids were placed both above and below the arm, thus covering an optimal surface area.

Joint torques are also dependent on the task that is being performed and specificity of training [42][43]. This should be kept in mind during the data collection process for experiments involving participants with abnormal movement patterns.

Contraction levels of both extensors and flexors are reflected in the EMG activation level. Participants were also asked to contract their muscles upto 10% of the maximum possible voluntary contraction. The activation and muscle forces of the flexors was comparatively higher than that of the extensors. Literature dictates that the flexor muscles are generally stronger than extensor muscles in healthy subjects as is predicted by [44]. The standard deviations are high in the stroke patient data and this could have been due to involuntary muscle spasticity and less muscle forces during the tasks [45].

EMG driven musculoskeletal models have been adopted in many studies for the estimation of individual muscle forces. Validation of torque and joint moments has been done by comparing the experimentally recorded or predicted torques with the one estimated by the model. The inverse dynamics routine often puts accuracy in jeopardy as it involves numerical differentiation of the joint position data. Any movement artifacts in the input data could potentially influence the derivative values [8]. This problem is averted in this study as joint torques were recorded experimentally as well, and have been directly used as an input to the calibration block of the modeling pipeline.

In [46], HD-EMG recordings were decomposed using CKC to extract MU firing rate information from the finger muscles in stroke patients. It was

found that the MU firing rate was significantly reduced in stroke patients over examined force levels of 2 to 10 N, which could be attributed to changes in intrinsic properties of spinal motor neurons. However, the application of CKC decomposed HD-EMG in studies of stroke patients with a focus on wrist muscles is still rather limited and needs to be addressed more urgently.

The proposed methodology is novel on its own as HD-EMG is included in the modeling pipeline, and torque validations were performed on stroke participants in this study. The model used in the study also assumed a non-linear relationship between EMG and force. This is a step ahead of the linear relationship assumption of EMG and force which has been found to overestimate activation levels of muscles [8]. However, this methodology also has some limitations. First of all, calibration of the model parameters is a sensitive step in the process of torque estimation and could always be improved. The only tasks set for the stroke participants were wrist flexion and extension, therefore calibration of the model was done on two trials of the same tasks. Moreover, six muscles are taken into consideration instead of all the muscles spanning the wrist and hand. The wrist model used in this study was also scaled manually, using scale factors calculated from segment lengths of the forearm and hand that were also recorded manually. The scale factors would have been comparatively more accurate if a static file (.trc) of the subjects were used which would also take the mass of the segments into account. Manual intervention might have given rise to uncertainties in the measurement and scaling process. A lot of factors such as ability to achieve target MVC, responsiveness to tasks are also very subject and investigator dependent which could give rise to inconsistencies.

Additionally, when all trials of a participant were compared, it was found that the torque estimations made by the model had lower R and RMSE values for trials with comparatively higher flexion-extension activity. This was because the two trials used for calibration of the model as well as the other trials of the participant had comparatively similar ranges of EMG activity, joint position and experimental torques. It would be interesting to pursue a solution to this in future studies. In this study, all three extensor muscles are equally activated and all three flexor muscles are equally activated. Two filtered cumulative trains were used to activate all six muscles, such that all extensors were activated by the extension EMG train and all flexors by the flexion EMG train. Therefore, the results could have been improved by including more specific muscle excitations and activations. There is no golden standard or the best method for surface EMG normalization, especially for dynamic tasks [47]. [48] and [49] suggest using EMGs from MVC as the normalization reference. HD-EMG signals of each trial were normalized by the maximum EMG amplitude among all eight trials,in case of both flexion and extension. Additionally, it would be interesting to explore the outcome of different EMG normalization routines in HD-EMG driven musculoskeletal modeling.

Wrist torque comparison - healthy vs. stroke patients

Wrist torques are reported to be around 0.35 N.m for ADL, with a maximum of about 20 N.m [50]. In Table III, findings from wrist literature for healthy participants recorded under isokinetic conditions were compared with the overall average of maximal wrist torques of experimental stroke data and model estimations. The torque and range of motion values (Appendix E) reported in this study seem to be lower than that for healthy participants as reported in [51][50]. This could be due to a range of factors such as spasticity in stroke patients, different experimental conditions and positions of the wrist during each of the studies. It has been

Torques (in N.m)	**Wrist dynamics**		
	Healthy	**Stroke**	
		Experimental	**Estimated**
Wrist Flexion	8-9	4.2	3.9
Wrist Extension	5-6	3	2.96

Table III: Wrist dynamics - healthy vs. stroke patient data

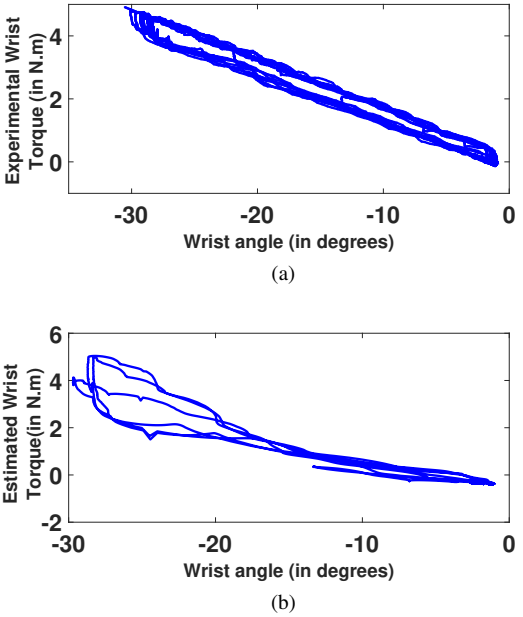

Figure 10: Maximal experimental and model wrist torques for stroke participants seen at extreme flexion angles for a representative trial are given by figures 10a and 10b respectively

established in [51] and [44], that in healthy participants, wrist torque in the flexion direction is significantly higher than the torque in the extension direction. Table III shows an agreement between this prediction in healthy patient literature and experimental/estimated wrist torques from stroke patients in this study. [51] also proved that under dynamic conditions maximal wrist torque occurred during extreme flexion/extension of the wrist in healthy participants. Experimental and estimated torque data is investigated and one representative trial can be seen in Figure 10 which agrees to these findings as well.

Lastly, CKC decomposed HD-EMG for the wrist muscles is still a very novel area and very limited research exists to validate and compare stroke patient data with healthy patient data specifically for the wrist. The healthy patient data borrowed from literature might have had different experimental and task settings as compared to the settings the stroke patients were recorded in. It would also be interesting to know the stiffness estimates computed by the model, and if there is significant difference in these estimates for healthy and stroke participants. Appendix C has a stiffness computation method that can be used to continue this study.

V. Conclusion

Stroke is one of the leading causes of adult disability, and significantly affects quality of life. This study looked into torque and model parameter estimation via HD-EMG driven musculoskeletal modeling in case of stroke participants. Results show that for stroke participants, the model estimated parameters and joint torques were well-correlated with the experimental torques in terms of shape and magnitude. Findings from this study can be applied to understand neuromechanical modeling strategies of the wrist and in the design of rehabilitation procedures for the wrist in stroke patients.

Future scope of project

An extension of this study could be carried out, where healthy patient data could be recorded in experimental conditions similar to the one reported in the study. Investigations on ranges of motion and wrist torque estimates could be compared better then. Healthy patient data reported in this study was adopted from existing literature where studies had different experimental settings, assumed different neutral positions of the wrist and were task specific in some cases. Moreoever, calculating the stiffness estimates of the wrist in case of stroke participants could bolster the understanding of neuromuscular dysfunctions in stroke patients. A comparison of these estimates with those of healthy participants would result in better prosthetic designs and wrist rehabilitation measures.

VI. Acknowledgements

I would like to thank dr. Massimo Sartori for defining, and supervising this Master Thesis assignment. I am extremely grateful to my daily supervisor Guillaume Durandau, who helped me in each stage of this project. I would also like to thank the rest of my graduation committee, prof. Bart Koopman and dr. Utku Yavuz for their valuable feedback and advice. I would like to thank dr. Ales Holobar for allowing us to work on experimental data recorded by him. I would also like to thank Christopher Pablo Cop for allowing me to train with his test data which helped me prepare for my project.

References

[1] K. Manal, R. V. Gonzalez, D. G. Lloyd, and T. S. Buchanan, "A real-time emg-driven virtual arm", *Computers in biology and medicine*, vol. 32, no. 1, pp. 25–36, 2002.

[2] L.-Q. Zhang, H.-S. Park, and Y. Ren, "Shoulder, elbow and wrist stiffness in passive movement and their independent control in voluntary movement post stroke", in *2009 IEEE International Conference on Rehabilitation Robotics*, IEEE, 2009, pp. 805–811.

[3] V. Squeri, L. Masia, P. Giannoni, G. Sandini, and P. Morasso, "Wrist rehabilitation in chronic stroke patients by means of adaptive, progressive robot-aided therapy", *IEEE transactions on neural systems and rehabilitation engineering*, vol. 22, no. 2, pp. 312–325, 2013.

[4] M. Asghari, S. Behzadipour, and G. Taghizadeh, "A planar neuro-musculoskeletal arm model in post-stroke patients", *Biological cybernetics*, vol. 112, no. 5, pp. 483–494, 2018.

[5] Q. Shao, D. N. Bassett, K. Manal, and T. S. Buchanan, "An emg-driven model to estimate muscle forces and joint moments in stroke patients", *Computers in biology and medicine*, vol. 39, no. 12, pp. 1083–1088, 2009.

[6] M. Sartori, M. Maculan, C. Pizzolato, M. Reggiani, and D. Farina, "Modeling and simulating the neuromuscular mechanisms regulating ankle and knee joint stiffness during human locomotion", *Journal of neurophysiology*, vol. 114, no. 4, pp. 2509–2527, 2015.

[7] K. Manal, K. Gravare-Silbernagel, and T. S. Buchanan, "A real-time emg-driven musculoskeletal model of the ankle", *Multibody system dynamics*, vol. 28, no. 1-2, pp. 169–180, 2012.

[8] T. K. Koo and A. F. Mak, "Feasibility of using emg driven neuromusculoskeletal model for prediction of dynamic movement of the elbow", *Journal of electromyography and kinesiology*, vol. 15, no. 1, pp. 12–26, 2005.

[9] J. Fernandez and M. Pandy, "Integrating modelling and experiments to assess dynamic musculoskeletal function in humans", *Experimental physiology*, vol. 91, no. 2, pp. 371–382, 2006.

[10] M. A. Lemay and P. E. Crago, "A dynamic model for simulating movements of the elbow, forearm, and wrist", *Journal of biomechanics*, vol. 29, no. 10, pp. 1319–1330, 1996.

[11] J. W. Ramsay, B. V. Hunter, and R. V. Gonzalez, "Muscle moment arm and normalized moment contributions as reference data for musculoskeletal elbow and wrist joint models", *Journal of biomechanics*, vol. 42, no. 4, pp. 463–473, 2009.

[12] P. Pigeon, L. Yahia, and A. G. Feldman, "Moment arms and lengths of human upper limb muscles as functions of joint angles", *Journal of biomechanics*, vol. 29, no. 10, pp. 1365–1370, 1996.

[13] W. M. Murray, S. L. Delp, and T. S. Buchanan, "Variation of muscle moment arms with elbow and forearm position", *Journal of biomechanics*, vol. 28, no. 5, pp. 513–525, 1995.

[14] G. Ettema, G. Styles, and V. Kippers, "The moment arms of 23 muscle segments of the upper limb with varying elbow and forearm positions: Implications for motor control", *Human Movement Science*, vol. 17, no. 2, pp. 201–220, 1998.

[15] S. L. Delp, F. C. Anderson, A. S. Arnold, P. Loan, A. Habib, C. T. John, E. Guendelman, and D. G. Thelen, "Opensim: Open-source software to create and analyze dynamic simulations of movement", *IEEE transactions on biomedical engineering*, vol. 54, no. 11, pp. 1940–1950, 2007.

[16] M. Damsgaard, J. Rasmussen, S. T. Christensen, E. Surma, and M. De Zee, "Analysis of musculoskeletal systems in the anybody modeling system", *Simulation Modelling Practice and Theory*, vol. 14, no. 8, pp. 1100–1111, 2006.

[17] O. Röhrle, U. Ş. Yavuz, T. Klotz, F. Negro, and T. Heidlauf, "Multiscale modeling of the neuromuscular system: Coupling neurophysiology and skeletal muscle mechanics", *Wiley Interdisciplinary Reviews: Systems Biology and Medicine*, e1457,

[18] P. Yao, D. Zhang, and M. Hayashibe, "Simulation of tremor on 3-dimentional musculoskeletal model of wrist joint and experimental verification?", in *2012 Annual International Conference of the IEEE Engineering in Medicine and Biology Society*, IEEE, 2012, pp. 4823–4826.

[19] J. A. Nichols, M. S. Bednar, S. J. Wohlman, and W. M. Murray, "Connecting the wrist to the hand: A simulation study exploring changes in thumb-tip endpoint force following wrist surgery", *Journal of biomechanics*, vol. 58, pp. 97–104, 2017.

[20] R. Merletti, A. Holobar, and D. Farina, "Analysis of motor units with high-density surface electromyography", *Journal of electromyography and kinesiology*, vol. 18, no. 6, pp. 879–890, 2008.

[21] A. Holobar, M. A. Minetto, and D. Farina, "Accurate identification of motor unit discharge patterns from high-density surface emg and validation with a novel signal-based performance metric", *Journal of neural engineering*, vol. 11, no. 1, p. 016 008, 2014.

[22] G. Drost, D. F. Stegeman, B. G. van Engelen, and M. J. Zwarts, "Clinical applications of high-density surface emg: A systematic review", *Journal of Electromyography and Kinesiology*, vol. 16, no. 6, pp. 586–602, 2006.

[23] A. Holobar and D. Zazula, "Multichannel blind source separation using convolution kernel compensation", *IEEE Transactions on Signal Processing*, vol. 55, no. 9, pp. 4487–4496, 2007.

[24] H. R. Marateb, K. C. McGill, A. Holobar, Z. C. Lateva, M. Mansourian, and R. Merletti, "Accuracy assessment of ckc high-density surface emg decomposition in biceps femoris muscle", *Journal of neural engineering*, vol. 8, no. 6, p. 066 002, 2011.

[25] Y. Ning, X. Zhu, S. Zhu, and Y. Zhang, "Surface emg decomposition based onk-means clustering and convolution kernel compensation", *IEEE journal of biomedical and health informatics*, vol. 19, no. 2, pp. 471–477, 2015.

[26] M. Sartori, U. Ş. Yavuz, and D. Farina, "In vivo neuromechanics: Decoding causal motor neuron behavior with resulting musculoskeletal function", *Scientific reports*, vol. 7, no. 1, p. 13 465, 2017.

[27] G. Durandau, D. Farina, and M. Sartori, "Robust real-time musculoskeletal modeling driven by electromyograms", *IEEE transactions on biomedical engineering*, vol. 65, no. 3, pp. 556–564, 2018.

[28] A. Nikooyan, H. Veeger, P. Westerhoff, B. Bolsterlee, F. Graichen, G. Bergmann, and F. van der Helm, "An emg-driven musculoskeletal model of the shoulder", *Human Movement Science*, vol. 31, no. 2, pp. 429–447, 2012, Special issue on Network approaches in complex environments, ISSN: 0167-9457. DOI: https://doi.org/10.1016/j.humov.2011.08.006. [Online]. Available: http://www.sciencedirect.com/science/article/pii/S016794571100145X.

[29] D. Farina, I. Vujaklija, M. Sartori, T. Kapelner, F. Negro, N. Jiang, K. Bergmeister, A. Andalib, J. Principe, and O. C. Aszmann, "Man/machine interface based on the discharge timings of spinal motor neurons after targeted muscle reinnervation", *Nature Biomedical Engineering*, vol. 1, no. 2, p. 0025, 2017.

[30] M. Sartori, G. Durandau, S. Došen, and D. Farina, "Robust simultaneous myoelectric control of multiple degrees of freedom in wrist-hand prostheses by real-time neuromusculoskeletal modeling", *Journal of neural engineering*, vol. 15, no. 6, p. 066 026, 2018.

[31] J. Oblak, I. Cikajlo, and Z. Matjacic, "Universal haptic drive: A robot for arm and wrist rehabilitation", *IEEE transactions on neural systems and rehabilitation engineering*, vol. 18, no. 3, pp. 293–302, 2009.

[32] D. G. E. Robertson and J. J. Dowling, "Design and responses of butterworth and critically damped digital filters", *Journal of Electromyography and Kinesiology*, vol. 13, no. 6, pp. 569–573, 2003.

[33] M. D. Djurić-Jovičić, N. S. Jovičić, and D. B. Popović, "Kinematics of gait: New method for angle estimation based on accelerometers", *Sensors*, vol. 11, no. 11, pp. 10 571–10 585, 2011.

[34] A. Seth, J. L. Hicks, T. K. Uchida, A. Habib, C. L. Dembia, J. J. Dunne, C. F. Ong, M. S. DeMers, A. Rajagopal, M. Millard, *et al.*, "Opensim: Simulating musculoskeletal dynamics and neuromuscular control to study human and animal movement", *PLoS computational biology*, vol. 14, no. 7, e1006223, 2018.

[35] C. Pizzolato, D. G. Lloyd, M. Sartori, E. Ceseracciu, T. F. Besier, B. J. Fregly, and M. Reggiani, "Ceinms: A toolbox to investigate the influence of different neural control solutions on the prediction of muscle excitation and joint moments during dynamic motor tasks", *Journal of biomechanics*, vol. 48, no. 14, pp. 3929–3936, 2015.

[36] M. Sartori, M. Reggiani, D. Farina, and D. G. Lloyd, "Emg-driven forward-dynamic estimation of muscle force and joint moment about multiple degrees of freedom in the human lower extremity", *PloS one*, vol. 7, no. 12, e52618, 2012.

[37] K. R. Saul, X. Hu, C. M. Goehler, M. E. Vidt, M. Daly, A. Velisar, and W. M. Murray, "Benchmarking of dynamic simulation predictions in two software platforms using an upper limb musculoskeletal model", *Computer methods in biomechanics and biomedical engineering*, vol. 18, no. 13, pp. 1445–1458, 2015.

[38] D. A. Winter, *Biomechanics and motor control of human movement*. John Wiley & Sons, 2009.

[39] T. S. Buchanan and D. G. Lloyd, "Muscle activity is different for humans performing static tasks which require force control and position control", *Neuroscience Letters*, vol. 194, no. 1-2, pp. 61–64, 1995.

[40] F. M. Colacino, R. Emiliano, and B. R. Mace, "Subject-specific musculoskeletal parameters of wrist flexors and extensors estimated by an emg-driven musculoskeletal model", *Medical engineering & physics*, vol. 34, no. 5, pp. 531–540, 2012.

[41] D. Staudenmann, I. Kingma, D. F. Stegeman, and J. H. van Dieën, "Towards optimal multi-channel emg electrode configurations in muscle force estimation: A high density emg study", *Journal of Electromyography and Kinesiology*, vol. 15, no. 1, pp. 1–11, 2005.

[42] W. L. Kenney, J. H. Wilmore, and D. L. Costill, *Physiology of sport and exercise*. Human kinetics, 2015.

[43] T. S. Buchanan, M. J. Moniz, J. P. Dewald, and W. Z. Rymer, "Estimation of muscle forces about the wrist joint during isometric tasks using an emg coefficient method", *Journal of biomechanics*, vol. 26, no. 4-5, pp. 547–560, 1993.

[44] M.-C. Jung and M. S. Hallbeck, "The effect of wrist position, angular velocity, and exertion direction on simultaneous maximal grip force and wrist torque under the isokinetic conditions", *International Journal of Industrial Ergonomics*, vol. 29, no. 3, pp. 133–143, 2002.

[45] X. L. Hu, K.-y. Tong, R. Song, X. J. Zheng, and W. W. Leung, "A comparison between electromyography-driven robot and passive motion device on wrist rehabilitation for chronic stroke", *Neurorehabilitation and neural repair*, vol. 23, no. 8, pp. 837–846, 2009.

[46] X. Li, A. Holobar, M. Gazzoni, R. Merletti, W. Z. Rymer, and P. Zhou, "Examination of poststroke alteration in motor unit firing behavior using high-density surface emg decomposition", *IEEE Transactions on Biomedical Engineering*, vol. 62, no. 5, pp. 1242–1252, 2014.

[47] A. Nikooyan, H. Veeger, P. Westerhoff, B. Bolsterlee, F. Graichen, G. Bergmann, and F. Van der Helm, "An emg-driven musculoskeletal model of the shoulder", *Human movement science*, vol. 31, no. 2, pp. 429–447, 2012.

[48] R. Merletti, W. Wallinga, H. Hermens, and B. Freriks, "Guidelines for reporting semg data", *Roessingh Research and Development*, pp. 101–105, 1999.

[49] H. J. Hermens, B. Freriks, R. Merletti, D. Stegeman, J. Blok, G. Rau, C. Disselhorst-Klug, and G. Hägg, "European recommendations for surface electromyography", *Roessingh research and development*, vol. 8, no. 2, pp. 13–54, 1999.

[50] A. J. McDaid, "Development of an anatomical wrist therapy exoskeleton (aw-tex)", in *2015 IEEE International Conference on Rehabilitation Robotics (ICORR)*, IEEE, 2015, pp. 434–439.

[51] J. L. Morse, M.-C. Jung, G. R. Bashford, and M. S. Hallbeck, "Maximal dynamic grip force and wrist torque: The effects of gender, exertion direction, angular velocity, and wrist angle", *Applied Ergonomics*, vol. 37, no. 6, pp. 737–742, 2006.

[52] L. Ombregt, "Applied anatomy of the wrist, thumb and hand", 2013.

VII. Appendix

A. Anatomical background of the wrist joint

The wrist joint is a complex mechanical and functional structure. It consists of carpal bones arranged in two rows. The scaphoid, lunate, triquetral and pisiform bones are found in the proximal row, whereas the trapezium, trapizoid, capitate and hamate bones form the distal row. It is a condyloid joint, its design permits flexion, extension, abduction and adduction. The radio-carpal joint is primarily responsible for movements of the wrist along two axes, and carries out wrist flexion-extension. Ulnar and radial deviation takes place along the anteroposterior axis. Wrist flexion and extension occurs along the transverse axis. Collateral palmar and dorsal ligaments restrict movements around the wrist. The dorsal ligaments are thin in comparison, and are aligned in the same axis as the forearm. The palmar ligaments on the other hand join the carpal bones to the radius and ulna, and remain taut during wrist extension. In this section, the anatomy of the wrist is elaborated from the point of view of applied anatomy and movement biomechanics.

Wrist flexion and extension have a range of motion of 85°though that range can be different for patients with spasticity. This is seen in the data from the stroke patients used for this project where the flexion-extension range was approximately 45°for flexion and extension separately. The amplitudes of radial and ulnar deviation for healthy participants is approximately 15°and 45°respectively. However, radial and ulnar deviation is considered to have significantly lesser clinical importance. The neutral position of the wrist is typically defined when it is held between flexion and extension.

Out of all the muscles and tendons that bind the wrist joint in place, three flexors and three extensors were included in this study. All wrist extensors can be found in the dorsal aspect of the wrist, whereas all flexors can be found in the palmar aspect of the wrist.

The extensor carpi radialis longus (ECRL) and the extensor carpi radialis brevis (ECRB) are innervated by the radial nerve. ECRL brings about wrist dorsiflexion in conjunction with the extensor carpi ulnaris (ECU), and radial deviation in conjunction with the flexor carpi radialis (FCR) muscle. The ECRB muscle is capable of extending the wrist, and bringing it back to the neutral position from ulnar deviation. The extensor function of the ECU is secondary and it mainly functions as a primary ulnar deviator of the wrist [52].

The main function of the FCR is wrist flexion and radial deviation. The flexor carpi ulnaris (FCU) works in conjunction with the FCR to flex the wrist. FCU and the ECU also work together to bring about ulnar deviation. FCR and FCU are innervated by the median and ulnar nerves respectively. The palmar longus muscle is another major muscle involved in palmar wrist flexion, however, it is absent in 15% of individuals and has not been included in the model.

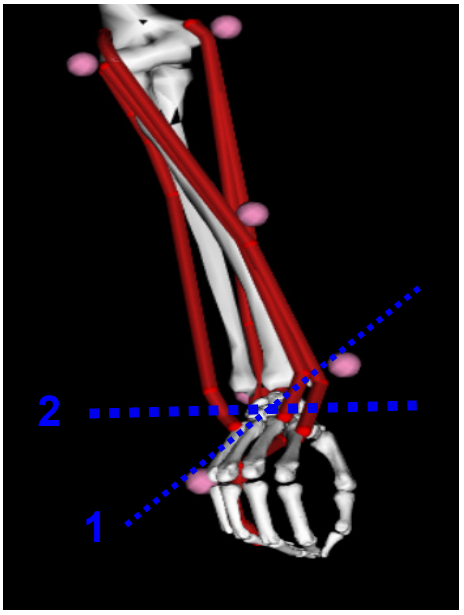

Figure A1: Musculoskeletal model of the wrist in neutral position. 1 is the anteroposterior axis, the direction of ulnar/radial deviation. 2 is the transverse axis along which flexion-extension occurs. Adapted from [52]

B. Processing Procedures

OpenSim 3.3, CEINMS and Matlab 2017 were used for offline processing of data.

OpenSim Model - data modeling

The MoBL ARMS dynamic model was modified on OpenSim to include the six muscles, ECRL, ECRB, ECU, FCR, FCU, FDSR, and one degree of freedom, wrist flexion-extension. The experimental joint position data was loaded as motion into the OpenSim model as .mot files. Visual checks were done to make sure the motion of the wrist was as expected, the position of the hand was also changed to replicate experimental conditions, such that the elbow flexion and pronation-supination coordinates were at 90°each in the input .mot file. The flexion and deviation coordinate values were obtained from experimental files. Figure A2 represents the scaling process.

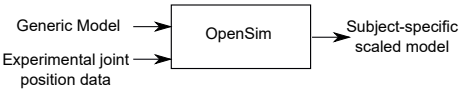

Figure A2: Schematic of the scaling process

Preparation of files for HD-EMG driven simulations

Custom made Matlab functions were used to create .mot inverse kinematics files, .sto inverse dynamics files and .mot EMG excitation files required for CEINMS.

Muscle Analysis (OpenSim)

The OpenSim model was scaled using manual scale factors derived from each subject's anatomical landmark location. Muscle analysis was run using this scaled model and the inverse kinematics file obtained from experimental joint position data. The Analyze Tool option was used on OpenSim to perform a muscle analysis for each trial of every patient. The same six muscles were chosen for muscle analysis, and moment arms for flexion and deviation were calculated using the analyze tool too. Finally, the output files of muscle tendon lengths of all muscles, and moment arms of flexion were used going forward. Figure A3 represents muscle analysis on OpenSim

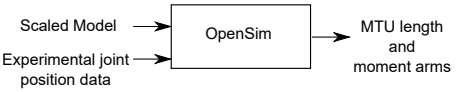

Figure A3: The scaled model and experimental joint position data are put into the model to get MTU length and flexion moment arms

Model Calibration (CEINMS)

The model's parameters were calibrated using EMG data, inverse kinematics and inverse dynamics. Three parameters were of primary importance while characterize the activation dynamics of the muscles; tendon slack length, muscle optimal fiber length, and a strength coefficient which tunes the maximum isometric force of the muscle.An open loop optimization routine minimizes the difference between the experimental and estimated torques.Figure A4 gives a schematic of how the calibrated model is obtained from CEINMS.

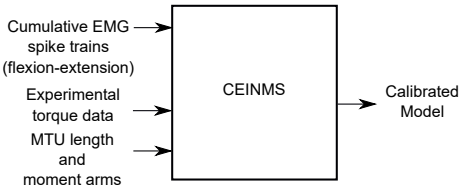

Figure A4: Schematic of the calibration input and outputs

Forward Dynamics using the HD-EMG driven model (CEINMS)

The calibrated model, along with the moment arms and MTU lengths, as well as EMG data were used to obtain the muscle variables and estimate joint torque data. The muscle variables of importance were; activations, muscle forces fiber lengths and fiber velocities. Figure A5 represents the parameter estimation process.

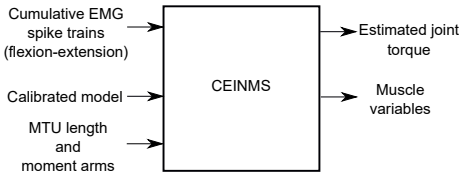

Figure A5: Schematic of CEINMS parameter estimation process

Cycle averages

Torque levels were validated for each individual trial of a participant and across participants. For each participant, an average of all cycles in every trial was taken from minimum to minimum. On average, four cycles were taken for each trial. An average of all cycles were taken for the trial and errors were calculated between experimental and estimated torques. For each participant, an average of all trials for that participant was also taken using the same logic. Once again, errors were calculated to see how much the estimated and experimental torques changed in case of each participant.

C. Stiffness computation for the wrist

Muscle variables such as flexion moment arms and MTU lengths can be used to derive wrist stiffness estimations for the stroke participants. Muscle stiffness, K^m is estimated as the partial derivative of muscle fiber force F^m with respect to the normalized fiber length, l^m.

$$K^m = \frac{\partial F^m(\alpha, l^m, v^m)}{\partial v^m} \tag{2}$$

Wrist stiffness can be estimated on Matlab using equation 2 and already existing, customized Matlab functions. The joint muscle names included in the OpenSim model have to be defined and assigned an identification value. In our case, the joint muscle names would be named ECRL, ECRB, ECU, FCU, FCR, FDSR and would have identity values from 1-6 serially. Following this, splines can be generated for activation length,α , normalized fiber length,l^m and normalized fiber velocity, v^m and moment arms. A inverse kinematic routine can be carried out for each trial to get the entire range of motion, and the degrees of freedom should be defined. Once these pre-requisites are done, CEINMS output files such as normalized fiber length, pennation angle, optimal fiber length, tendon slack length and strength coefficients of muscles can be used, for every trial to estimate wrist stiffness. Figure A6 gives a pictorial representation of the inputs and outputs during stiffness computation for the wrist. Healthy and stroke patient data are also assumed

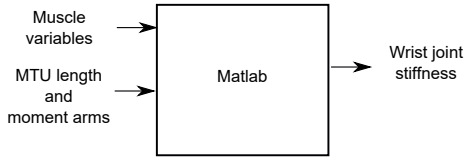

Figure A6: Muscle variables, MTU lengths and moment arms are the inputs which help in the estimation of wrist stiffness

to have significant differences, with spastic wrists having stiffness greater than 20Nm/rad [50].

D. Motor unit behaviour investigation in stroke patients

Progressive changes in intrinsic muscle mechanical properties and muscle structures are seen in paretic-spastic muscles post stroke. Transynaptic spinal MU degeneration, disuse, loss of central MU trophic influences could be one of the many factors behind these phenomena. Investigations on changes in MU behaviour and function post stroke help identification of factors that result in the deterioration of muscle strength and activity [46]. Subsequently, it could also help in guiding treatment and rehabilitation strategies.

Future versions of this study too, could focus on understanding how HD-EMG decomposition outcomes differ for healthy and stroke participants in case of wrist muscles.

E. Wrist range of motion - stroke vs. healthy patients

The flexion/extension angle is limited to $90°(\pm 45°)$ in the stroke patient data. It should be of note here that all stroke patient data was recorded with the UHD which may have significantly affected the allowable ranges of wrist flexion/extension angles. Table IV compares the ranges seen in experimental stroke patient data to healthy patient data from literature. The maximum wrist torque

Wrist motion	**Range of motion**	
	Healthy	Stroke (Experimental)
Flexion	65-80°	18-35°
Extension	55-75°	12-25°

Table IV: Wrist ranges of motion - healthy vs. stroke patient data

was limited to 10 N.m in the stroke patient data used in this study. Experimental maximal flexion torque values were in the range of 3.5-5.3 N.m whereas maximal model flexion torque estimates were in the range of 3-5 N.m. Experimental maximal extension torques ranged from 2-4 N.m and maximal model extension torque estimates were in the range of 2-3.5 N.m.

F. Flexion averages of all trials for each participant

The flexion averages were calculated for all cycles of each trial for every participant. For all participants, calibration was done for two trials and the calibrated model was extrapolated to all trials of that participant.

1) Flexion averages - Participant 1

Figure A7 represents all trials for participant 1. The R and RMSE values and standard deviations of both experimental torque and estimated torque was calculated for all trials. Figure A7a has the first trial with R and RMSE values of 0.0029 N.m and 0.947 respectively. R and RMSE values for Figure A7b, the second trial, are 0.2662 N.m and 0.9169 respectively. The third trial is given by Figure A7c and has an RMSE value of 0.2659 N.m and R value of 0.9544. The model was calibrated using trials four and five. The RMSE of the fourth trial given by Figure A7d is 0.1050 N.m and this trial has an R value of 0.9555. Figure A7e represents the fifth trial, and has an RMSE value of 0.1708 N.m and R value of 0.9888. Figure A7f has RMSE and R values as 1.0650 and 0.9663, respectively. Figure A7g has a comparatively higher RMSE value of 5.3036 N.m and an RMSE of 0.1095. Finally, the eight trial as per Figure A7h has an RMSE of 2.8092 N.m and an R value an of 0.7633. The last two trials, trial seven and nine have very high torques in comparison to the other trials even though their joint position and EMG data is comparable to the other trials. Therefore, for these two trials the model estimated torque is not as good as that for the other trials.

2) Flexion averages - Participant 2

Figure A8 shows plots of all trials for participant 2. The R and RMSE values and standard deviations of both experimental torque and estimated torque was calculated for all trials. The first trial (Figure A8a) has R and RMSE values of 0.0403 N.m and 0.9273 respectively. The model was calibrated using trials four and five. R and RMSE values for the fourth trial (Figure A8b) are 0.6616 N.m and 0.9809 respectively. Figure A8c represents the fifth trial and has an RMSE value of 0.3077 N.m and R value of 0.8943. The RMSE of trial six (Figure A8d) is 0.8781 N.m and this trial has an R value of 0.9653.

3) Flexion averages - Participant 3

Figure A9 shows plots of all trials for participant 3. The R and RMSE values and standard deviations of both experimental torque and estimated torque was calculated for all trials. The fourth trial had to be excluded from this study as there was no experimental EMG extension activity in this trial.

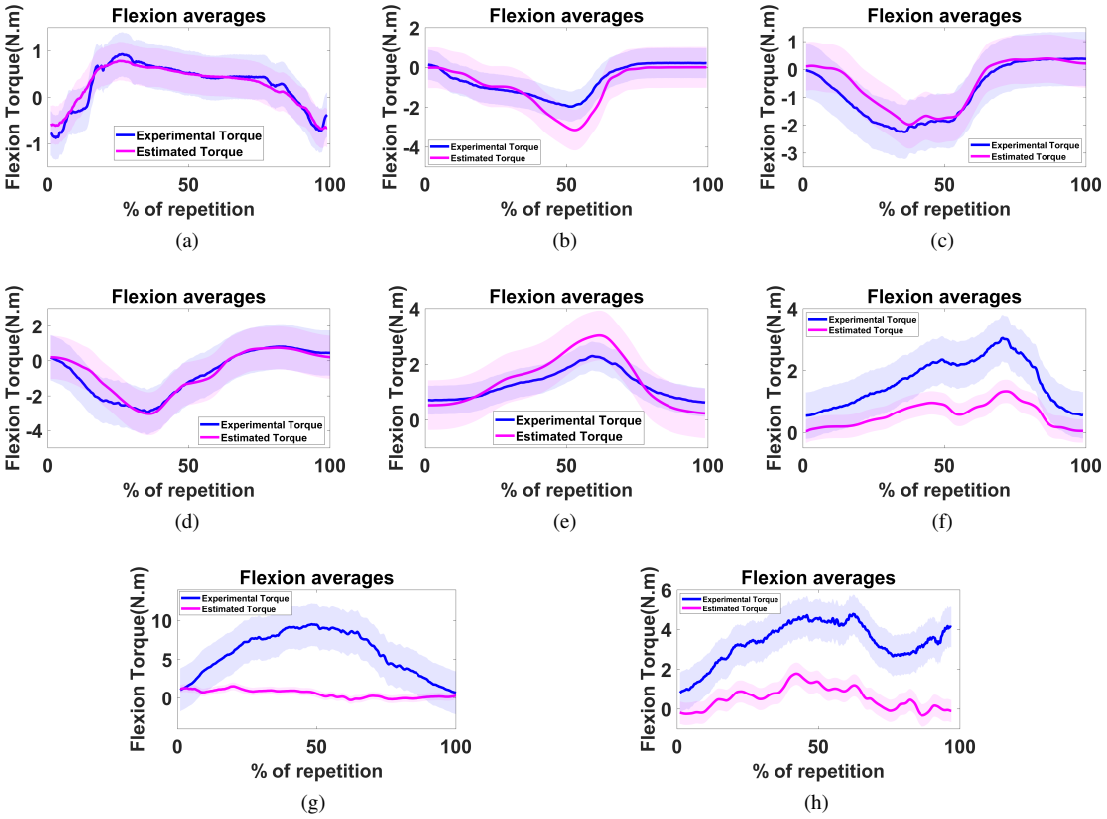

Figure A7: Flexion averages of all trials of participant 1. The thick blue line represents the experimental torque whereas the thick magenta line represents the estimated torque. The shaded area gives the standard deviation of the experimental and estimated torques

The model was calibrated using trials three and six. Trial three, Figure A9a has R and RMSE values of 0.3380 N.m and 0.9446 respectively. R and RMSE values for the fifth trial, Figure A9b are 0.7201 N.m and 0.8905 respectively. The sixth trial, Figure A9c has an RMSE value of 0.6641 N.m and R value of 0.9746. The RMSE of the seventh trial, Figure A9d is 0.8498 N.m and this trial has an R value of 0.9668. The final trial number 8, given by Figure A9e has an RMSE and R value of 1.56 N.m and 0.9688 respectively.

4) Flexion averages - Participant 5

Figure A10 shows plots of all trials for participant 5. The R and RMSE values and standard deviations of both experimental torque and estimated torque was calculated for all trials. The model was calibrated using trials three and four. The third trial (Figure A10a) has R and RMSE values of 0.2527 N.m and 0.9626 respectively. R and RMSE values for the fourth trial (Figure A10b) are 0.1496 N.m and 0.9051 respectively. Figure A10c represents the fifth trial and has an RMSE value of 0.0640 N.m and R value of 0.9786. The RMSE of trial six (Figure A10d) is 0.5140 N.m and this trial has an R value of 0.3326. The sixth trial for this participant had extremely large ECRB muscle forces and the model estimated torque follows the pattern of the ECRB muscle entirely, giving deviant values in terms of shape and magnitude.

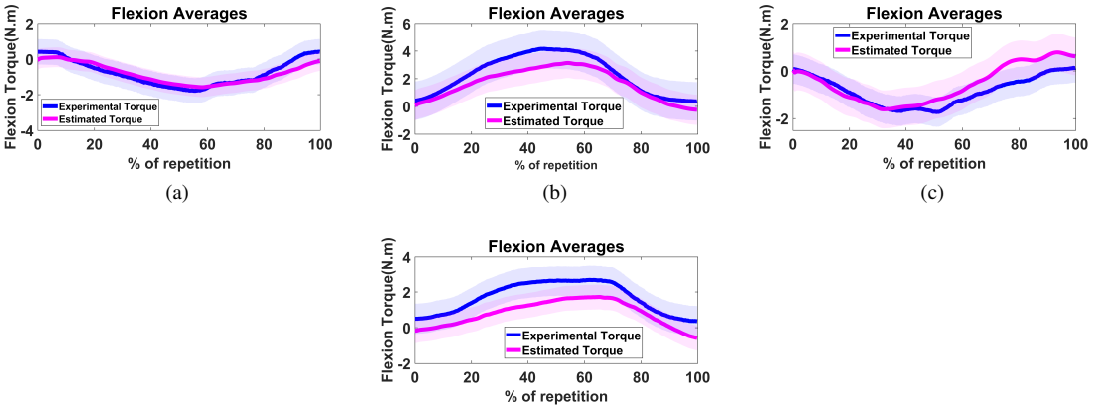

Figure A8: Flexion averages of all trials of participant 2. Blue and magenta lines represent experimental adn estimated torques respectively. The shaded area gives the standard deviation of the experimental and estimated torques

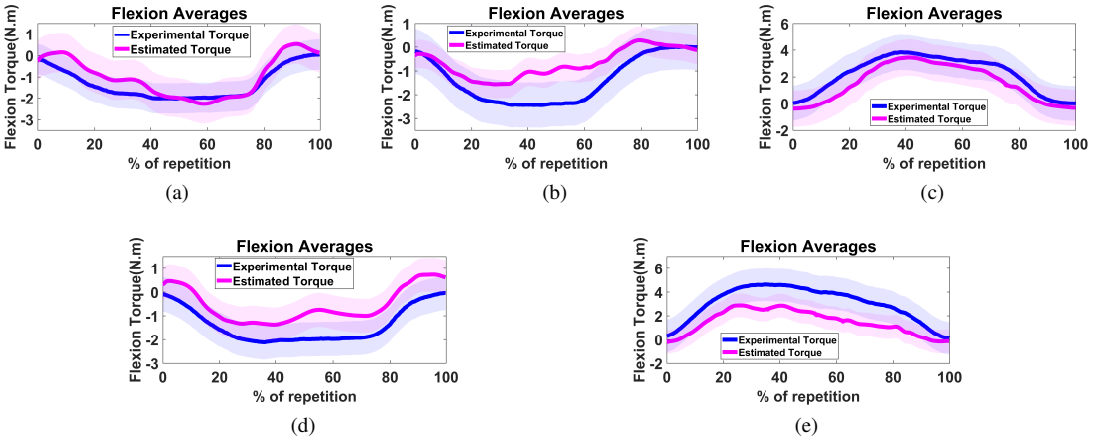

Figure A9: Flexion averages of all trials of participant 3. Blue and magenta lines represent experimental adn estimated torques respectively. The shaded area gives the standard deviation of the experimental and estimated torques

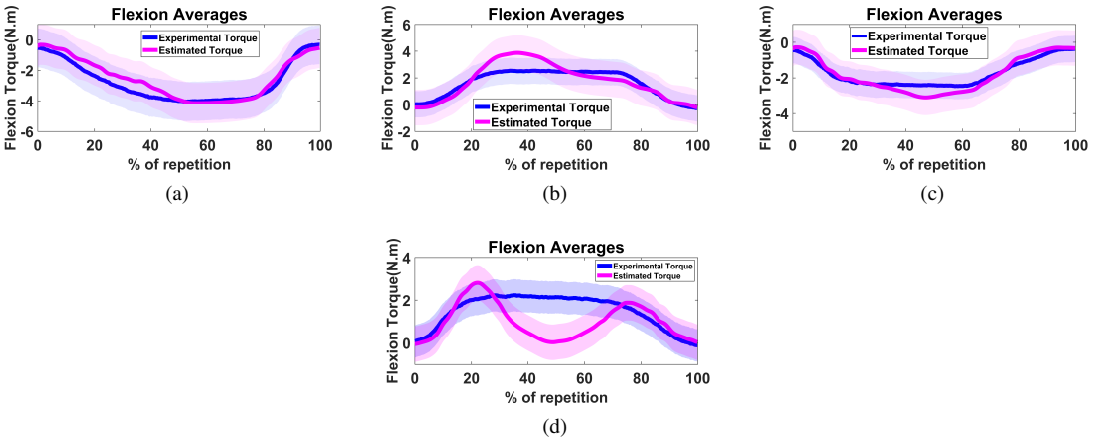

Figure A10: Flexion averages of all trials of participant 5. Blue and magenta lines represent experimental adn estimated torques respectively. The shaded area gives the standard deviation of the experimental and estimated torques